The Experimental Evaluation of Simple Bidirectional DC/DC Converter with Snubber Compensation for Electric Vehicle Application

Syifaul Fuada[1] and Braham Lawas Lawu[2]
[1] Program Studi Sistem Telekomunikasi, Universitas Pendidikan Indonesia, Bandung, Indonesia
[2] PT. Perusahaan Listrik Negara (PLN) UPP Kitring, Muara Taweh, Kalimantan Tengah, Indonesia
Email: syifaulfuada@upi.edu

***Abstract*—This research discusses the implementation of a buck-boost converter which is also known as a Bidirectional DC/DC Converter (BDC) in electric vehicles with a specific focus on electric All-Terrain Vehicles (ATV). The BDC circuit was used to integrate the main battery of the ATV (Li-Po) with the secondary battery (a 25V max./8 Farad Supercapacitor bank). This is to ensure the main battery of the ATV motor safer from unstable output load currents through the charging and discharging mechanism facilitated by BDC in order to ensure it has a longer lifetime. This discussion is more focused on the charging mechanism which occurs when the BDC is in buck mode (36V to 18 V). Meanwhile, the DC motor was used as the load inductor in this BDC circuit. It is also important to note that an interruption in the current flowing either due to a switch or other components has the ability to cause a voltage or current spike in the semiconductor switch component. Therefore, a special circuit was required to be connected to the main circuit to reduce interruption and also indicates the role of the snubber circuit in reducing the spike. This paper is more highlighted on voltage spike reduction. Moreover, LTSpice simulation was applied to verify the BDC circuit design, and the results obtained were compared with a real laboratory measurement based on the ability to change the Duty Cycle on the V_{out} of the BDC circuit for the charging mechanism. The determination of the desired V_{out} was followed by a change in the parameters of the BDC circuit such as input voltage, inductor value, switching frequency, duty cycle, and power supply configuration to determine their impact on the V_{out} of BDC, Spike, and MOSFET's temperature. The experiments showed that the Snubber circuit was able to compensate for voltage fluctuations in the MOSFET.**

***Index Terms*—All-terrain vehicles, bidirectional DC/DC converter, buck-boost converter, electrical vehicles, snubber circuit, supercapacitor**

I. Introduction

Mini-electric All-Terrain-Vehicles (ATV) is a type of electric four-wheeled vehicle used in areas which are difficult to be accessed by large vehicles [1]. They are massively produced using varying capacities of DC motors between 350-3000 Watt and battery as the power source. These DC motors have a minimum supply of voltage which varies from 36V to 42V depending on the power capacity. This means the energy required by the motor in the system is very fluctuating and has the ability to wear out quickly when the expensive Lithium type of battery is used as the only source of energy in the ATV. This means there is the need for a secondary or alternative energy source such as supercapacitors to ensure the battery has a longer lifetime and keep its performance more stable. The supercapacitor is expected to be used as a companion to the main energy supply which is the Lithium battery due to its several advantages such as fast charging and discharging processes and a large power density which allows it to overcome the problem of energy fluctuations required by the DC motors [2]–[4]. It is, however, important to note that an electronic circuit with a certain topology is needed to realize this battery-supercapacitor mechanism.

A buck-boost converter circuit or a Bi-directional DC/DC Converter (BDC) has been used in previous studies [5], [6] to integrate the battery into a supercapacitor but the discussion in [5] focuses more on the boost mode of BDC which is the discharging mechanism (18 V to 36 V) and buffering (maintaining at 36 V) while [6] focuses on the charging mechanism or the Buck mode. The 18 V is minimum voltage of the Supercapacitor while 36 V is the maximum voltage of the load (DC motor). This current research was, therefore, conducted as an extended version of [6] where the BDC circuit is added to a Snubber circuit to reduce voltage or current spikes in switching components. This snubber circuit generally consists of resistors, capacitors, and diodes.

II. State-of-the Art

Studies have been conducted on the use of BDC, both in simulation and hardware implementation, to integrate the main battery of electric vehicles into a supercapacitor as indicated by the proposals of B. Zhang *et al*. [7], V. Ivakhno *et al*. [8], K. Bhatt *et al*. [9], A.B. Culture & Z.M. Salameh [10], and C. Wang *et al*. [11]. In [7], the BDC circuit was modified by adding a diode into the main circuit to reduce voltage stress caused by the changes in the on to off condition at a very fast time on the switching component. The system was intended to be applied in the

Manuscript received October 12, 2021; revised December 18, 2021; accepted December 27, 2021.
Corresponding author: Syifaul Fuada (email: syifaulfuada@upi.edu).

doi: 10.18178/ijeetc.11.4.284-293

Generic Hybrid Energy Storage System (HESS) case with a battery/supercapacitor scheme and the mathematical calculations have been conducted carefully. However, the system was only verified in an ideal environment which is on MATLAB and Simulink but direct measurements need to be made on the hardware because real conditions are different from simulation. Moreover, BDC hardware has also been simulated and realized for high-power battery applications in [8] but the control process on the microcontroller is very complex due to the complicated topology which involved 10 IGBT and this means a special algorithm is needed in this case.

In [9], a BDC circuit equipped with a Snubber capable of producing an output voltage of up to 325V with an input voltage of up to 60V was applied to an electric vehicle but it also used a complicated topology which is an isolated type of BDC and dual-switch forward Snubber as observed in [8]. Furthermore, in [10], a basic BDC circuit without Snubber was developed for energy distribution applications from 24 V to 48 V using the PIC16F684 as the primary controller in the DC/DC converter system. In [11], a basic BDC circuit without Snubber was also applied in hybrid electric vehicles using an IGBT-Si MOSFET as the switching device. The research was more focused on changing the switching frequency & Duty Cycle to determine its effect on several aspects such as efficiency, output current, and temperature when the BDC circuit is in boost and buck mode in order to obtain the most ideal variable setting according to the needs in terms of these aspects.

Aditama *et al*. also modified buck-boost DC/DC converter to achieve higher output voltage and increase efficiency but the concrete application of the proposed system was not clearly investigated [12]. Moreover, Suwarno and Sutikno proposed a buck-boost converter to maintain the output voltage at 15 V even when the input voltage changes. The voltage stabilizer was, however, dedicated to Renewable Energy applications including Photovoltaic and Windpower, and not for electric vehicles [13]. Al-Qaisi *et al*. [14] and Darameičika *et al*. [15] later presented a DC/DC buck converter but they focused on a controller method such as Sliding Mode Controller (SMC) & Current Mode Controller (CMC) and this means the application of the proposed system is not clearly defined.

The objective of this current study is generally different from [7]–[11] as indicated by the differences in the application. A simple basic BDC circuit with a non-isolated topology was used for the Li-Po battery/supercapacitor ATV Motor scenario with the working range set at 18 to 36 V and an STM32F4 microcontroller used as the duty cycle controller. It is important to note that this microcontroller has been equipped with interface features on the computer through STMStudio by STMicroelectronics™ vendors to monitor the supercapacitor voltage, battery voltage, and supercapacitor charging process in real-time when the system is working. Moreover, a simple Snubber circuit consisting of one resistor, capacitor, and diode component was installed on each switching component while the LTSpice simulation approach was applied to verify the model before the BDC circuit was incorporated in the hardware. The experiments were conducted by changing certain variables to determine their effect on system performance in line with the method used in [11]. This was necessary to determine the most appropriate setting to produce output according to specifications but the focus was specifically on the Buck mode of the BDC.

III. Methods

A. Buck-Converter Mode Design

Buck converter is a type of DC/DC converter usually used to lower a certain voltage level as indicated in the general topology presented in Fig. 1.

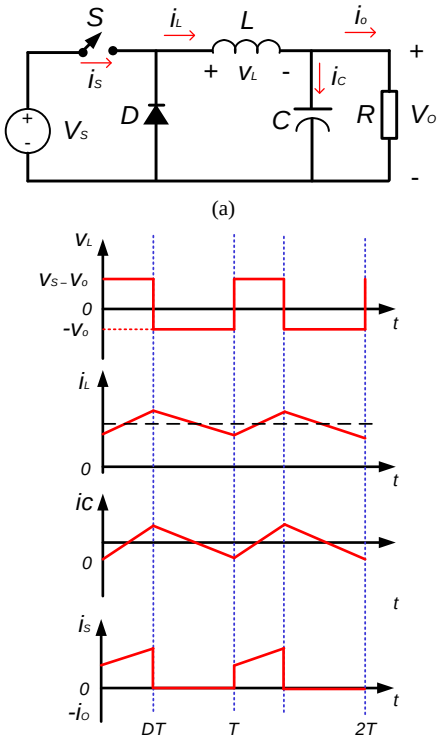

Fig. 1. Buck converter: (a) The basic configuration of the buck converter circuit and (b) buck converter waveform.

It is important to note that V_s is the input voltage of the converter and S is the symbol for the switching component while the diodes, capacitors, inductors, and loads are represented by D, C, L, and R respectively. Moreover, this Buck converter circuit has two possible modes concerning the current flowing in the inductor [16], [17] which are the Continuous Conduction Mode (CCM) where the current passing through the inductor is continuous and will never be 0 A as well as the Discontinuous Conduction Mode (DCM) where the current through the inductor is 0 A. The relationship between the output voltage (V_{Out}) and V_{in} (denotes as V_s) in this circuit can be written as (1) and it is possible to derive the duty cycle value from (1) as expressed in (2):

$$V_{Out} = \text{Duty Cycle} \times V_S \quad (1)$$

$$\text{Duty Cycle} = V_{Out} / V_S \quad (2)$$

For ensuring continuous mode the value of inductor designed must be greater than L_b, as expressed by (3):

$$L_b = \frac{(1-D)R}{2f} \tag{3}$$

It is important to note that the variable R denotes a load resistance which is 10 Ω and when the value of $L>L_b$, the buck converter will work in CCM mode. Moreover, the function of the capacitor as a filter in the buck converter needs to be limited in order to avoid large DC ripple voltage, and this means the value of the capacitor used should satisfy the following condition:

$$C > \frac{(1-D)V_{\text{Out}}}{8V_r Lf^2} \tag{4}$$

where V_r is the ripple voltage.

V_{in} value as the working voltage of the DC motor in the BDC circuit was 36 V while the supercapacitor used has a maximum voltage rating of 25 V but the desired voltage was 18 V. Moreover, the charging output current of the desired Supercapacitor (I_{out}) was 4 A and the duty cycle was set at 0.5 or 50% with reference to (2) while the frequency value was set to 10 kHz. Equations (3) and (4) were also used to set the minimum values for the inductor and capacitor at 112.5 µH and 55.55 µF respectively. These values (inductor and capacitor) were calculated using a 10 kHz of switching frequency. The gate driver IC TLP250F used in this work has a 25 kHz (max.) of switching frequency as informed by the datasheet. For this reason, 10 kHz is allowed. The voltage ripple used in this work is 1% of the voltage output (18 V) so that we obtained 0.18V.

B. System Description

Fig. 2 presents the circuit used in the experiment and it has several blocks including the BDC main circuit which contains several components as indicated in Table I, ATV's DC motor 36 V, Supercapacitor 25 V/8F, external boost converter module, and Li-Po Battery which are the same as those used in [5]. Moreover, the STM32F4 microcontroller was used to adjust the Switching Frequency (F_{sw}) with a Duty Cycle of 50% PWM, and the gate legs on S_1 and S_2 were connected to the microcontroller through an intermediary gate driver circuit (IC TLP250F).

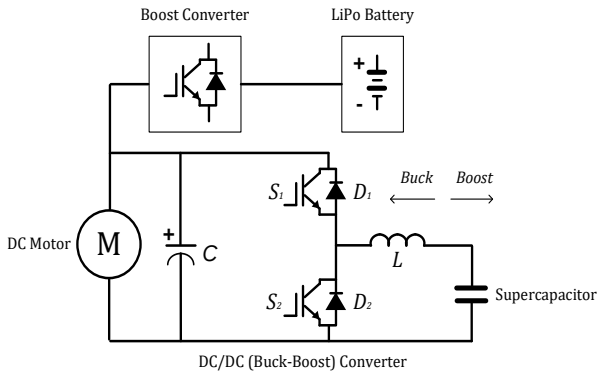

Fig. 2. BDC basic circuit, high-side = 36 V and low-side = 18 V

TABLE I. THE MAIN COMPONENTS IN THE BDC CIRCUIT

No	Components	Quantity	Description
1	Switching component (S_1 & S_2)	2	Power MOSFET P75NF75
2	Diode (D_1 & D_2)	2	MUR1560
3	Capacitor (C)	2	100 µF
4	Inductor (L)	1	Core PQ 2.5 Mh

The switching frequency (F_{sw}) used was selected according to the capability of the TLP250F IC at 10 kHz while the summary of the L and C calculations selected to be greater than the calculated results in Section III A is presented in Table I.

C. Feedback Design for Microcontroller ADC

A feedback circuit was needed to connect the BDC circuit to the Analog-to-Digital Converter (ADC) pin of the STM32F4 Microcontroller. It is important to note that there are two feedback circuits which are boost mode and Buck mode with the same circuit as indicated in Fig. 3. The pin was, therefore, used to measure the V_{out} of the BDC circuit which was desired to be 18 V in Buck mode with the maximum limit being 20 V. Meanwhile, the specifications showed the V_{in} of the STM32F4 Microcontroller ADC is 3 V. Therefore, the voltage was reduced from 20 V to 3 V using a voltage divider circuit as indicated in (5) which was further reduced to (6) to determine the combination of R_1 and R_2.

$$V_{\text{out}} = \frac{R_1}{R_1+R_2}V_{\text{in}} \tag{5}$$

$$\frac{V_{\text{out}}-V_{\text{in}}}{V_{\text{in}}} = \frac{R_2}{R_1} \tag{6}$$

where V_{In} = 20V and V_{Out} = 3V.

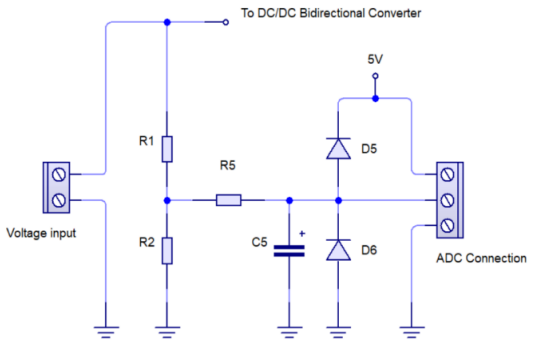

Fig. 3. ADC Feedback circuit to read BDC voltage in boost & buck mode.

The values of the V_{in} and V_{out} were inputted to obtain R_1 = 17 kΩ which requires two resistors, 15 kΩ and 2 kΩ, in series and R_2 = 3 kΩ. Meanwhile, R_5 = 22 Ω was used as the current limiter for the ADC pin of the STM32F4 Microcontroller while C_5 was applied to refine the ADC readings on the microcontroller because it forms a low-pass filter. Diodes D_5 and D_6 were used for safety, especially when the incoming voltage to the STM32F4 Microcontroller exceeds 3 V during the hardware implementation. It is also important to note that the components in boost mode are the same as buck mode but the calculation of the R_1 and R_2 is different due to the difference in the V_{in} value.

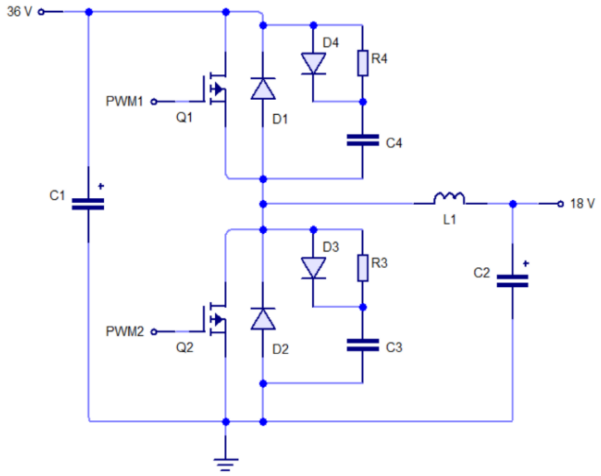

Fig. 4. BDC circuit connected to the snubber circuit.

D. Snubber Circuit Design

The presence of a switch or other component interfering with the current flow in a circuit with an inductor load has the ability to cause a voltage (*dv/dt*) or current (*di/dt*) spike in the switching component and this can interfere with the performance of other components in the circuit. The circuit overheats quickly and can be damaged when the current and voltage spikes are above the maximum limit of the switch component. It is, however, possible to solve this problem using a snubber circuit which also has the ability to safe switching components against stress during the transition from "on" to "off" conditions or vice versa. This stress occurs due to the incomplete current cut off when the voltage starts to rise which has the ability to damage the switch components [18]. Fig. 4 shows a snubber circuit connected to the BDC main circuit.

The snubber circuit consists of resistors, diodes, and capacitors, each of which has a special function. The resistors block current and reduce temporary voltage spikes in switching circuits, capacitors reduce the existing transient current by slowing down the discharge of stored electric charge due to the inability of the voltage on the capacitor to change instantly while the diodes accelerate the deceleration process of the capacitor due to their fast reverse recovery or on to off time. The resistors (R_4 & R_3) and capacitors (C_3 & C_4) were calculated using (7) and (8), respectively. Moreover, the working voltage of the BDC circuit is in the range of 18 V to 36 V and the assumption of voltage spike in the switching circuit up to 3 times the maximum BDC voltage (36 V) is expected to increase the value to 108 V. Therefore, the instantaneous maximum spike voltage was set at 100 V.

$$R_{\text{snub}} = \frac{E_{\text{out}}}{I_{\text{out}}} \tag{7}$$

where DC source output (E_{out}) was set at 100 V and current output (I_{out}) limitation was 4A according to specifications and this means Resistor for Snubber circuit (R_{snub}) is 25 Ω. However, the resistor was not available in the market and this led to the use of 22 Ω during the implementation process.

$$C_{\text{snub}} = i_c \frac{dt}{dv} \tag{8}$$

where i_c is the maximum current through the capacitor which was 4 A according to specifications while the *dt* was 62.5 µs based on measurements on the oscilloscope and dv was 100 V and Capacitor for Snubber circuit (C_{snub}) was calculated to be 2.5 µF. Moreover, the snubber diodes (D_3 & D_4) were selected based on the consideration of voltage rating, current flow, and reverse recovery time (50 ns) capability. The results from the calculations are summarized in Table II.

TABLE II: COMPONENTS IN THE SNUBBER CIRCUIT

No	Components	Quantity	Description
1	Resistor (R_{snub}) which is R_3 and R_4	2	22 Ω
2	Diode (D_{snub}) which is D_3 and D_4	2	HER305
3	Capacitor (C_{snub}) which is C_3 and C_4	2	2.5 µF

IV. RESULTS

A. Simulation Using LTSpice

The BDC circuit was first modeled on LTSpice using the specified parameters as indicated in Fig. 5 before the hardware was produced and the values of C_{in} = C_{out} = 100 µF and L = 2.5 mH were obtained. Moreover, the ideal parameters of the MUR1560 diode and P75NF75 MOSFET were inputted into the simulation according to the datasheet with the MOSFET provided a voltage source (V_2 and V_3) as PWM and the switching frequency set to 10 kHz with 50% duty cycle. It is important to note that the snubber circuit was not included in the simulation because all the components were considered to have ideal values.

A block diagram is produced in Fig. 6 and connected to a voltage of 36 V and an 8 Farad Supercapacitor as indicated in Fig. 5. The simulation results showed that the V_{out} value is as expected which is ~18 V (17.17342 V to be exact) with an average current of 1.7055 A and an RMS current of 1.7327 A. This means the V_{out} has the ability to charge the 8 Farad supercapacitor with a maximum voltage rating of 25 V in this buck mode.

TABLE III: THE EFFECT OF CHANGING THE DUTY CYCLE ON THE BDC OUTPUT VOLTAGE IN THE SIMULATION

No	Duty cycle	V_{out}
1	0.3	9.951765 V
2	0.4	13.566124 V
3	0.5	17.17342 V
4	0.6	20.722794 V

Moreover, the duty cycle values were varied as shown in Table III to determine the effect of the variation on BDC's output voltage and the results showed that the calculation made using (2) is in line with the design. Using PWM 30%, the V_{out} produces ~9.9 V. The higher Duty Cycle, the higher V_{out}. This was observed with the increment in the V_{out} when the duty cycle was increased to 60% and vice versa. It was also discovered that 50% duty cycle is more suitable considering the fact that the gap it produced is larger to achieve both high and low voltage.

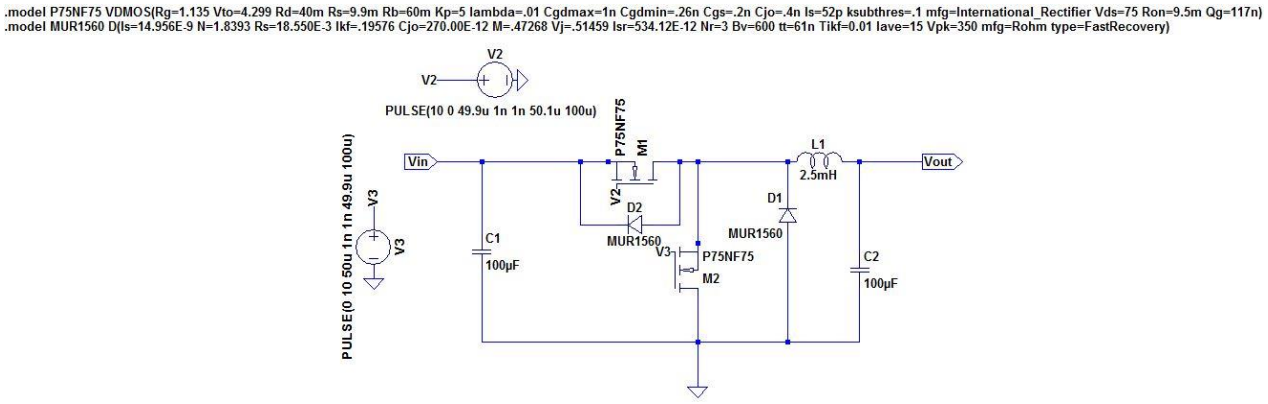

Fig. 5. Buck mode BDC circuit configuration in LTSPice simulation.

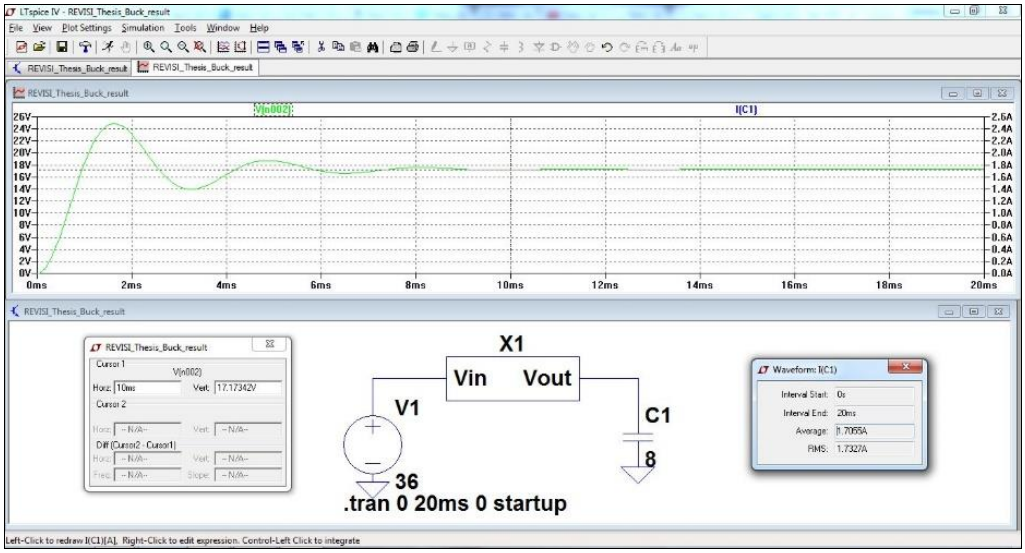

Fig. 6. Simulation results of buck mode bidirectional DC/DC converter circuit.

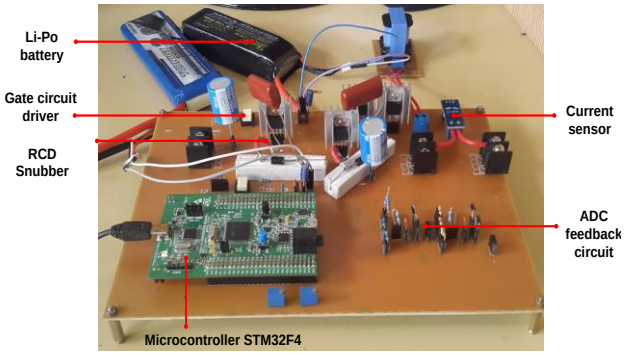

Fig. 7. PCB of the BDC circuit.

TABLE IV: ITEMS REQUIRED FOR SYSTEM TESTING

No	Components	Quantity	Description
1	Current sensor	2	ACS712
2	Supercapacitor *bank*	-	Specification25 V / 8F
3	External module DC/DC boost converter	1	Set from 22.2 V to 36 V
4	Power supply	3	Battery Li-Po 11.1V 2200mAh
5	PWM Controller	1	Microcontroller STM32F4 Discovery
6	Gate driver	2	IC TLP250F

B. Hardware Implementation and Performance Measurement

The hardware produced is presented in Fig. 7 with the PCB observed to contain several blocks including the BDC circuit, space for the Microcontroller, Gate driver MOSFET, ADC feedback as well as the input and output pins. The Snubber circuit is mounted directly on the P75NF75 Power MOSFET leg while the other items included were required for testing purposes as presented in Table IV.

The system was specifically tested for buck mode and this involved the connection of two 11.1V 2200 mAh Li-Po batteries in series to produce a voltage of 22.2 V which was later increased using a DC/DC boost converter module to 36 V which was used as the V_{in} for the BDC circuit. Moreover, the switching frequency and duty cycle settings were adjusted to 10 kHz and 50% respectively according to the calculations and simulations while the Gate driver circuit was supplied with a voltage of 11.1 V which is a single supply method. The experimental setup of the test is presented in Fig. 8 (a) with the BDC circuit connected to a PC with STMStudio installed while Fig. 8 (b) indicates the measurement of the voltage across the capacitor when the BDC circuit is in buck mode.

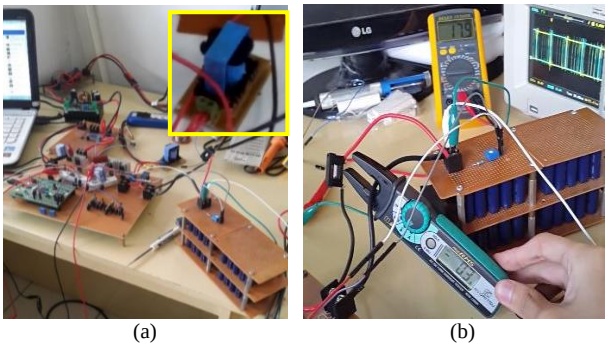

(a) (b)

Fig. 8. (a) Experimental setup, reproduced from [6], (b) Measurement of the output voltage at BDC when in Buck mode (charging Supercapacitor) with V_{in} = 36 V to obtain V_{out} = 17.9 V/3A

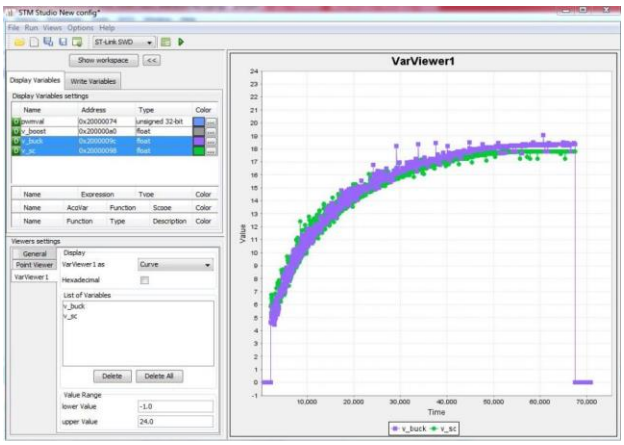

Fig. 9. The plot of charging voltage on supercapacitor using STMStudio. In the plot, when t=0 to t<=4, the voltage on the supercapacitor is immediately filled from 0 V to 4.5 V at a duration of approximately 3 seconds. Furthermore, from t<=4 to t>=50, the voltage reached the desired 18 V.

The results showed that the supercapacitor charging test was conducted successfully with the BDC circuit observed to have functioned effectively in buck mode as indicated in Fig. 9. The real-time plotting on the STMStudio also showed the system is capable of charging Supercapacitors up to 18 V. Moreover, the hardware used was in normal temperatures (not warm nor hot), especially both P75NF75 MOSFETs and MUR1560 diodes. Even though the temperature of the input capacitors (C_1 & C_2) slightly increased, it was within reasonable limits. The snubber circuit also had a warm temperature, especially in the resistor section which experienced power dissipation due to voltage spikes on the drain-source of the P75NF75 MOSFET but the spike was minimal at <5 V.

TABLE V: EFFECT OF CHANGING DUTY CYCLE ON BDC OUTPUT VOLTAGE OF THE HARDWARE

No	Duty cycle	V_{out}
1	0.3	10.5 V
2	0.4	13.9 V
3	0.5	17.9 V
4	0.6	21.6 V

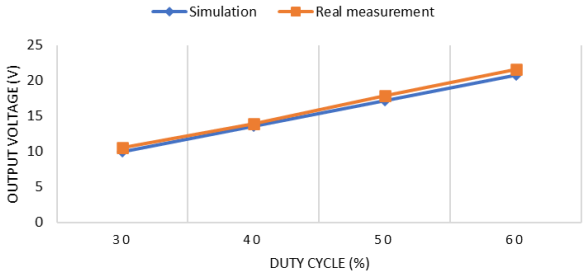

Fig. 10. Comparison graph of V_{out} of the BDC circuit in simulation and real-life condition.

The PWM values were also varied in the LTSpice simulation as shown in Table V to determine the effect of changing the Duty Cycle on BDC's voltage output and the results showed that the V_{out} increased when the duty cycle was increased to 60% and vice versa.

Fig. 10 compares the BDC simulation on LTSpice which is the ideal condition with the hardware which indicates real condition and a non-significant difference was recorded due to the non-ideal factor of the component values used.

C. Experiment I

The determination of the most appropriate settings was followed by experimentation which involved changing the variables to determine the impact on the system performance. The parameters changed include 1) input voltage which was varied from 0 to 36 V, 2) inductor value, 3) switching frequency, 4) power supply configuration including dual and single supply, and 5) the use of Snubber circuit. The three main variables considered were 1) the output voltage (V_{out}) of the BDC with the focus on its response to the minimum-maximum limit of the Supercapacitor, 2) Spike with the focus on determining whether the voltage and current spike of the BDC circuit is within the tolerable level, and 3) the MOSFET's temperature to determine whether it is normal, warm, or hot during the charging conditions. It is important to note that 0.5 was used for the duty cycle in the experiment. The scenario setting is shown in Table VI.

TABLE VI: EXPERIMENTAL SETTING OF THE BUCK MODE OF BDC CIRCUIT

Parameters	**Final result**	**Experiment 3**	**Experiment 2**	**Experiment 1**
V_{in} setup	Varied from 0 V to 36 V			
L (inductor)	2.5 mH	446 µH		
Switching frequency (F_{SW})	10 kHz	20 kHz	40 kHz	
Duty Cycle	0.5			
Supply Configuration	Single Supply	Dual Supply	Single Supply	
Snubber Installation	Yes		No	

The first scenario involved using an inductor which is smaller than the initial value with L = 2.5 mH changed to 446 µH which is a toroidal inductor type as shown in Fig. 11 (a). The real value of L was measured by LCR Meter (EXTECH model 380193). The switching frequency was also increased to 20 kHz while two voltage values from the Li-Po battery, +11.1 V and −11.1 V (dual supplies), were provided for the gate driver circuit. Moreover, the

input voltage was regulated from 0 V to 36 V by the Power Supply as indicated in Fig. 11 (b) and the results showed the BDC circuit produced a good output up to V_{in} = 18 V. Digital Multimeter (HELES UX866TR) was used to measure the voltage parameters. The shape of the drain-source signal from the MOSFET was also good and the maximum V_{out} value of the BDC circuit was recorded to be 8.9 V as presented in Fig. 11 (c). Meanwhile, it was necessary to increase the V_{out} by 10 V again to guarantee it has the ability to charge the supercapacitor.

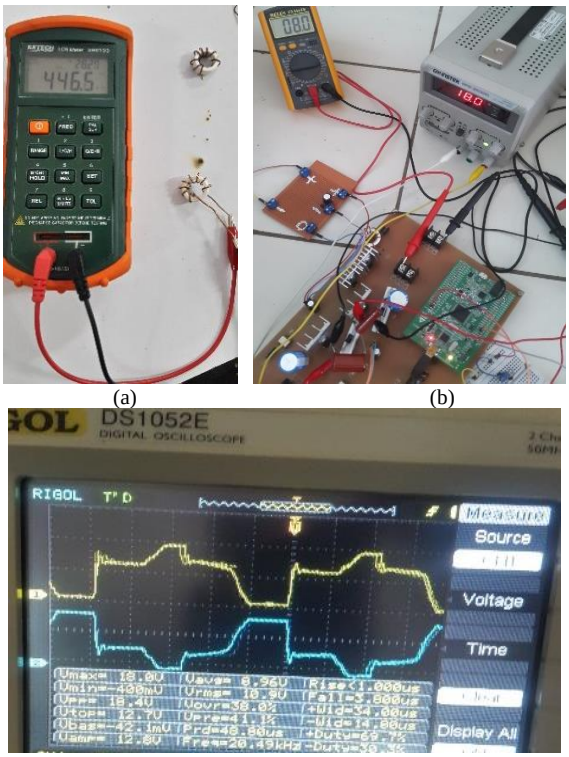

Fig. 11. (a) Measurement of the inductor used for the experiment I, (b) Experimental setup I, and (c) The drain-source MOSFET voltage on high-*side and low-side* at V_{in} = 18 V observed from RIGOL DS1052E Digital Oscilloscope.

The increment of the V_{in} to 36 V, however, increased the temperature of Power MOSFET P75NF75, C_1, and C_2 due to the fact that the MUR1560 diode was unable to conduct. This is associated with the use of a toroidal inductor with a ferrite core which is easy to saturate and a small number of turns usually produces a large inductance. It is, therefore, important to note that ferrite is not generally used as the base material for an inductor in a DC/DC converter circuit but an iron powder is normally applied as the basic material for the toroidal inductor. This means the inductor plays an important factor in producing a larger V_{out} and this was observed in the production of spikes greater than 5 V but below 10 V.

D. Experiment II

The inductor used in the second experiment was the same as the first experiment which was 446 µH but the switching frequency was increased to 40 kHz which was above the frequency capability of the gate driver IC TLP250F (25 kHz). Moreover, only one voltage or single supply which is +11.1 V was provided for the gate driver circuit from the Li-Po battery. The scenario setting is shown in Table VI.

The results showed the BDC circuit can only be used when V_{in} = 14 V and this stable value produced a maximum V_{out} value of 6.9 V as shown in Fig. 12 (a). This means it was necessary to increase the V_{out} by 11 V again to ensure it has the ability to charge the supercapacitor, which is about 18V. It was also discovered that the Drain-Source signal form of the MOSFET produced a high voltage spike which was almost 9 V as indicated in Fig. 12 (b), thereby, making the two MOSFETs, C_1, and C_2 warm. Moreover, V_{in} was increased from 14 V to 18 V and the MOSFET was shorted instead at a certain time due to the fact that the time fall on it was not fast enough to change from "on" to "off" when a PWM signal was applied.

This experiment shows that the switching frequency needs to be set below the maximum frequency of the Gate driver used in addition to the inductor value factor to produce better system performance. It is important to note that it is possible to first observe the specifications of the optocoupler in the Datasheet before determining the switching frequency setting on the Microcontroller.

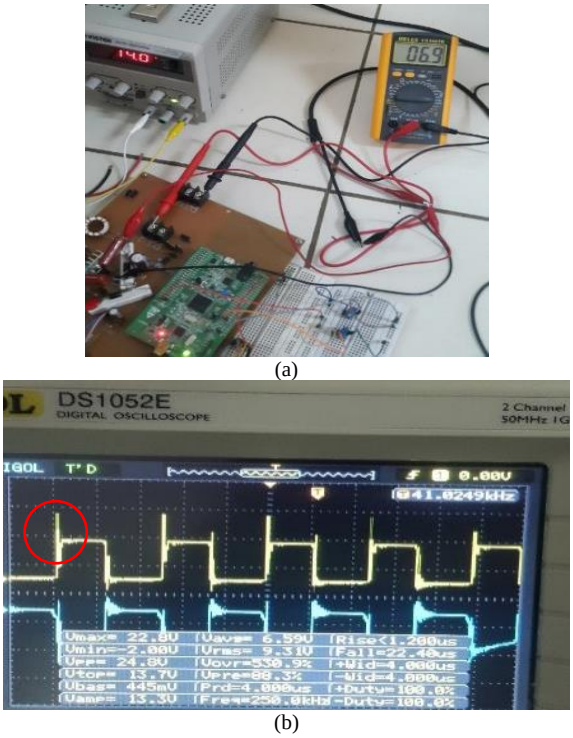

Fig. 12. (a) Experimental setup II, and (b) the drain-source MOSFET voltage on high-side and low-side at V_{in} = 14 V

E. Experiment III

The third experiment used a 446 µH inductor, 40 kHz switching frequency, single supply, and the Snubber circuit removed from the Drain & Source pin of the MOSFET. The result showed that the BDC circuit was only usable when V_{in} = 10 V and this produced V_{out} = 5 V. The scenario setting is shown in Table VI.

The Drain-Source voltage had a high spike which was approximately 23 V in both high-side and low-side

MOSFETs as indicated in Fig. 13 (a) and they were both shorted at a very fast time as indicated in Fig. 13 (b). In the first experiment, we used 10 V as an input voltage, and the given output and spike were 5 V and 23 V, respectively. For this reason, we need to reduce the spike voltage because we need to implement it for a higher input voltage, which is 36 V voltage, to get 18 V of output voltage. This, therefore, made both MOSFETs, C_1 and C_2 to have a hot temperature. The input voltage of 10V produced 23 V of output spike made us aware that 36 V of the input voltage will be applied; we expect that it would be more than 100 V spike output voltage given. This experiment showed that the Snubber circuit is also very influential in reducing voltage spikes in addition to the inductor value and switching frequency. The P75NF75 diode has a voltage slope of peak recovery (dv/dt) which is 12 V/ns as informed by the datasheet. The RIGOL DS1052E digital Oscilloscope used in this experiment has a specification that meets the proper requirement to measure dv/dt parameter of P75NF75; it can measure up to 200 ns.

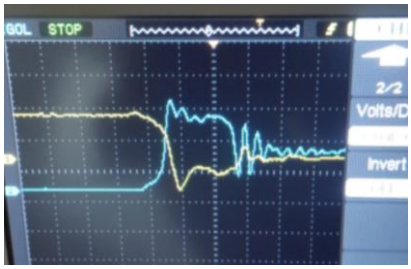

(a)

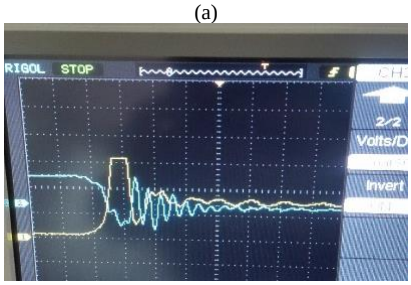

(b)

Fig. 13. (a) Experimental setup III, (b) The drain-source MOSFET voltage on high-side and low-side at V_{in} = 10 V.

The summary of the tests conducted on the system through experiments is presented in Table VI and the initial setting was found to be the most suitable. The specification of this setting are 1) 36 V to 18 V working voltage with the 18 V used to charge the supercapacitor and 36 V for the ATV's DC motor, 2) less than 5 V minimum spike, and 3) the temperature of the BDC components are within normal range.

Table VII shows the summary of the test. As we can see, the experiment I is the worst setting option compared to experiment II and experiment III because there is no Snubber circuit to compensate for the voltage spike of the BDC (>25V of the voltage spike). Experiment II uses high F_{SW} and small inductor value with a single supply for BDC, resulting in a high spike, and the V_{out} of BDC is low (only 5V to 10V). Experiment III uses dual supply resulting in a high spike, and the V_{out} of BDC is low, but the MOSFET temperature is still normal both at the high-side and low-side. The BDC cannot be applied for Supercapacitor/Battery integration when we use experiments II and III as the setting reference – this is because the Supercapacitor as V_{out} needs at least 18V. Later, the DC motor of ATV needs 36V with a very low spike to maintain the MOSFET temperature in normal condition. Therefore, we need induction input as high as possible, lower F_{SW} (fit with gate driver datasheet's recommendation), and proper snubber circuit installation.

The practical results of the snubber circuit addition were observed on the digital oscilloscope (RIGOL DS1052E) in a real-time setting. We compare the signal of "without" and after "with" snubber circuits following with the numerical values of the peaks during the switching time to expose the proposed circuit effects. Fig. 14 visualizes the measurement results: the snubber circuit can reduce the overvoltage peaks (from >23V to <10V). The observation result is shown in Table VIII; the 5th experiment was carried out to prove that there is a significant effect in the addition of the snubber circuit, which is to reduce V_{spike}. The setting is the same with 1st experiment to obtain valid data with equivalent comparison: V_{in} setup is varied from 0 V to 36 V, L = 446 µH, FSW = 40 kHz, Duty Cycle = 50%, single supply setting for supply configuration. A snubber circuit was installed for 5th experiment. With the same settings, the addition of the Snubber circuit made the MOSFET temperature normal compared to the 1st experiment. In addition, using the Snubber circuit, the V_{spike} was also proven to be derivable. However, the 5th experiment is not the best setting option because the output voltage of BDC circuit is still low, i.e., 5.1V. Some proper settings to achieve the desired goal refers to the final result scenario, as presented in Table VII.

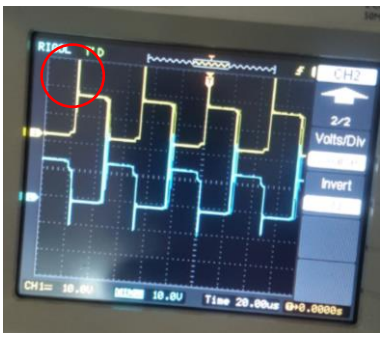

(a)

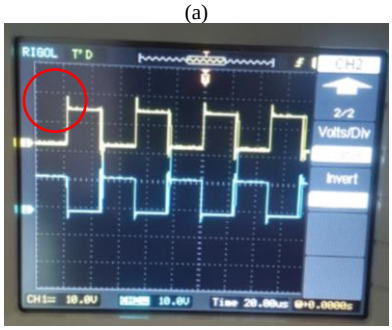

(b)

Fig. 14. Experimental setup to distinguish the effect of snubber circuit compensation with T/DIV = 20 µs and V/DIV = 10V for Channel 1 and Channel 2: (a) before (about >23 V of spike voltage) and (b) after (under 10V of spike voltage).

TABLE VII: EXPERIMENTAL RESULTS OF THE BUCK MODE OF BDC CIRCUIT IN DIFFERENT SETTING

Parameters	Final result	Experiment 3	Experiment 2	Experiment 1
V_{in} of BDC	Can be used up to 36 V	18 V max.	14 V max.	10 V max.
V_{out} of BDC	18 V	8.9 V	6.9 V	5 V
V_{spike}	<5 V	10 V <V_{spike}<5 V		>23 V
MOSFET temperature	Normal			High side (Buck) & Low side (Boost) of the BDC is heat
Result	The most fitted result	High spike, low V_{out}		Bad setting option

TABLE VIII: PRACTICAL RESULTS OF THE BDC "WITH" AND "WITHOUT" SNUBBER CIRCUIT INSTALLATION

Parameters	Experiment 1	Experiment 5 (additional experiment)
V_{in} of BDC	10 V max.	10 V max.
V_{out} of BDC	5 V	5.1 V
V_{spike}	>23 V	<10V
Snubber Installation	No	Yes
MOSFET temperature	High side (Buck) & Low side (Boost) of the BDC is heat	Normal

V. CONCLUSION

BDC circuits have been designed, simulated, and implemented for ATV applications but this study focused on the Buck mode which involves charging the 8F Supercapacitor which was rated at 25 V. It was discovered that the right configuration to produce V_{out} from BDC when buck mode is equal to 18 V and V_{in} is 36 V is to use 2.5 mH Inductor, 10 kHz switching frequency, 0.5% Duty cycle, single supply, and a Snubber. This configuration has the ability to produce the 18 V output required by the 8F Supercapacitor. Moreover, these settings also ensure the MOSFET temperature, input capacitor, and output capacitor are at room or normal temperature and also produced a low spike voltage which was under 5 V. The experiments conducted by changing the variables in the BDC circuit also proved that the inductor, Snubber circuit, and switching frequency have a significant influence on the performance of the system. However, it was impossible to calculate the Snubber installation from the beginning of the system design and this made it necessary to determine the working system by considering the MOSFET (variable *dv/dt*) through the Oscilloscope. This was due to the fact that the Spike can be used to calculate the R_{snub} and C_{snub} values. It is also important to note that the D_{snub} used was selected due to its high reverse recovery capability. Furthermore, it is possible to attach a fan to the system in addition to the use of a *heatsink* on the MOSFET to reduce the heat dissipated while the system is running. It is recommended to include the PID controller in the design so as to improve the transition state performance which is very crucial for safeguarding of Supercapacitor. The state space average model of the proposed system and control design as suggested in (4) will be also involved in the future publication.

CONFLICT OF INTEREST

The authors declare no conflict of interest.

AUTHOR CONTRIBUTIONS

S.F. conceptualized the topic, studied literatures in depth, defined the system specification, chosen the components and buy them, written/ English proof-edited/ layout edited this manuscript, worked on this project, analyzed the obtained data, validated the results, and funded the research. B.L.L conceptualized the topic, designed the system, designed the PCB, assembled the electronics components, collected the data, worked on this project, and performed the case study. All authors had approved the final version.

REFERENCES

[1] F. A. Rusu, G. Livint, and C. G. Pintilie, "Study of an Electric ATV by Removing the Thermal Engine," in *Proc. International Conference on Electromechanical and Energy Systems*, Craiova, Romania, Oct. 2019, pp. 1–4.

[2] L. Kouchachvili, W. Yaïci, and E. Entchev, "Hybrid battery/supercapacitor energy storage system for the electric vehicles," *J. Power Sources*, vol. 374, pp. 237–248, Jan. 2018.

[3] A. Tahri, H. E. Fadil, F. Z. Belhaj, *et al.*, "Management of fuel cell power and supercapacitor state-of-charge for electric vehicles," *Electr. Power Syst. Res.*, vol. 160, pp. 89–98, Jul. 2018.

[4] B. H. Nguyen, R. German, J. P. F. Trovao, and A. Bouscayrol, 'Real-time energy management of battery/supercapacitor electric vehicles based on an adaptation of Pontryagin's minimum principle," *IEEE Trans. Veh. Technol.*, vol. 68, no. 1, pp. 203–212, Jan. 2019.

[5] S. Fuada, B. L. Lawu, and B. K. Basavarajappa, "Buffering supercapacitor mechanism based on bidirectional DC/DC converter for mini all-terrain vehicle application," *Adv. Sci. Technol. Eng. Syst. J.*, vol. 5, no. 4, pp. 244–251, 2020.

[6] B. L. Lawu, S. Fuada, S. Ramadhan, A. F. Sabana, and A. Sasongko, "Charging supercapacitor mechanism based-on bidirectional DC-DC converter for electric ATV motor application," in *Proc. Int. Symposium on Electronics and Smart Devices (ISESD)*, Yogyakarta, Oct. 2017, pp. 129–132.

[7] B. Zhang, Z. Zhang, D. Wang, P. Li, and Y. Rong, "A bi-directional DC/DC converter for battery-supercapacitor hybrid energy storage system," *Electrotech. Electron. Autom*, vol. 68, no. 2, pp. 5–13, 2020.

[8] V. Ivakhno, V. Zamaruiev, B. Styslo, and A. Blinov, 'Experimental verification of a two-stage bidirectional DC/DC converter with separated commutation and asymmetrical structure of current-source stage," *Lviv*, Ukraine, Jul. 2019, pp. 369–374.

[9] K. Bhatt, R. A. Gupta, and N. Gupta, "Design and development of isolated snubber based bidirectional DC–DC converter for electric vehicle applications," *IET Power Electron.*, vol. 12, no. 13, pp. 3378–3388, Nov. 2019.

[10] A. B. Cultura II and Z. M. Salameh, "Design and analysis of a 24 V to 48 V bidirectional DC-DC converter specifically for a distributed energy application," *Energy Power Eng.*, vol. 4, no. 5, pp. 315–323, 2012.

[11] C. Wang, R. Xiong, H. He, X. Ding, and W. Shen, "Efficiency analysis of a bidirectional DC/DC converter in a hybrid energy storage system for plug-in hybrid electric vehicles," *Appl. Energy*, vol. 183, pp. 612–622, Dec. 2016.

[12] R. D. N. Aditama, N. Ramadhani, J. Furqani, A. Rizqiawan, and P. A. Dahono, "New bidirectional step-up DC-DC converter derived from buck- boost DC-DC converter," *Int. J. Power Electron. Drive Syst.*, vol. 12, no. 3, pp. 1699-1707, Sep. 2021.

[13] S. Suwarno and T. Sutikno, "Implementation of buck-boost converter as low voltage stabilizer at 15 V," *Int. J. Electr. Comput. Eng. IJECE*, vol. 9, no. 4, Aug. 2019.

[14] M. A. F. Al-Qaisi, M. A. Shehab, A. Al-Gizi, and M. Al-Saadi, "High performance DC/DC buck converter using sliding mode controller," *Int. J. Power Electron. Drive Syst.* vol. 10, no. 4, pp. 1806-1814, Dec. 2019.

[15] M. Darameičikas F. M. Sukki, S. H. A. Bakar, *et al.*, "Improved design of a DC-DC converter in residential solar photovoltaic system," *Int. J. Power Electron. Drive Syst.*, vol. 10, no. 3, pp. 1476-1482, Sep. 2019.

[16] C. Bai, B. Han, and M. Kim, "A bidirectional switch based half-bridge series-resonant converter operating in DCM and CCM," in *Proc. of 2020 IEEE Applied Power Electronics Conference and Exposition*, 2020.

[17] S. Wibowo, M. Facta, and A. Nugroho, "Operasi DC-DC konverter tipe cuk dengan mode DCM & CCM dengan transistor Sc2555 sebagai saklar," *Transient*, vol. 4, no. 2, pp. 261–267, 2015.

[18] K. Ahadi, "Design of 12 Volt 60 ampere buck converter using P-channel MOSFET and IGBT type N'," *Ketenagalistrikan Dan Energi Terbarukan*, vol. 11, no. 1, pp. 53–66, 2012.

Syifaul Fuada obtained a B.A. degree in electrical engineering education from Universitas Negeri Malang (UM), Indonesia and M.Sc. degree in microelectronics option of electrical engineering from the School of Electrical Engineering and Informatics, Institut Teknologi Bandung (ITB), Indonesia. He was with the University Center of Excellence at Microelectronics ITB from 2016-2018 as a main studyer. He is presently with the Program Studi Sistem Telekomunikasi Universitas Pendidikan Indonesia (UPI) as a Lecturer. His study interests include analog circuit design and instrumentation, circuit simulation, engineering education, IoT, multimedia learning development, and Visible Light Communication.

Braham Lawas Lawu received B.Eng. degree on electrical engineering from Maranatha Christian University in 2014 and Microelectronics option of Electrical Engineering from the School of Electrical Engineering and Informatics, Institut Teknologi Bandung (ITB), Indonesia, in 2017. He is presently with the PT. Perusahaan Listrik Negara (PLN) UPP Kitring, Muara Taweh, Barito Utara, Kalimantan Tengah. His work interests include Analog Instrumentation and Measurement, Analog Integrated Circuit Design, Power Electronics, and Embedded Systems.